Proceedings

The Emergence of Microneedle-based Smart Sensor/Drug-Delivery Patches: A Scaling Theory Defines the Trade-off between Response Time and Limits of Detection

Marco Fratus [1] and Muhammad A. Alam [1]*

[1] Elmore Family School of Electrical and Computer Engineering, Purdue University,West Lafayette, IN 47907 USA; mfratus@purdue.edu, alam@purdue.edu
* Correspondence: alam@purdue.edu

Abstract: Smart, ultra-scaled, always-on wearable, and implantable (WI) sensors are an exciting frontier in personalized medicine. These sensors integrate sensing and actuation capabilities, enabling real-time analyte detection for on-demand drug delivery, akin to a biological organ. The microneedle (MN)-based patch serves as a critical novel interface element in this system. It is inexpensive, minimally invasive, and safe, showing promise in glycemic management and insulin therapy in laboratory and animal studies. However, the current design of MNs relies primarily on empirical approaches, with significant challenges. These challenges include potential diffusion delays that may impede time-critical drug intervention and an iterative design process lacking a clear understanding of the trade-off between response time and limits of detection. In this paper, we introduce the first predictive framework for MN sensors, based on physical scaling laws and biomimetic concepts. Our framework is supported by experimental and numerical validations, establishing analytical scaling relationships that capture the fundamental workings of hollow and porous-swellable MN sensors. It quantifies essential performance metrics like "response time (RT)" and "limit of detection (LOD)" while assessing trade-offs associated with various geometrical and physical parameters of the MN technology. As a result, our model provides a universal framework for interpreting/integrating experimental findings reported by laboratories worldwide. By leveraging this predictive framework, researchers can advance the development and optimization of MN sensors, leading to improved performance and expanded applications in the field of wearable and implantable technologies.

Keywords: wearable and implantable sensors; modeling; scaling; microneedle; amperometry; response time; sensitivity; limit of detection; mechanics of insertion.

Citation: Fratus, M.; Alam, M.A. The Emergence of Microneedle-based Smart Sensor/Drug-Delivery Patches: A Scaling Theory Defines the Trade-off between Response Time and Limits of Detection. *Journal Not Specified* **2022**, *1*, 0. https://doi.org/

Received:
Accepted:
Published:

1. Introduction

Smart healthcare, powered by ultra-scaled, always-on digital electronics and wearable and implantable (WI) sensors, marks an exciting frontier in modern medicine. Technological advancements, including microfabrication, miniaturization, portability, low power, and cost-effectiveness, have shifted testing sites from traditional laboratories to "under or on skin" platforms [1–4].

Traditional devices developed for laboratory-based measurements face inherent limitations [5]: expensive tests, limited access in poorer communities, obtaining a single data point per test, and significant delays related to sample collection, laboratory reports, and therapy. Despite promoting point-of-care (POC) diagnostics as a complementary approach, these limitations persisted, hindering independent and continuous monitoring of chronic diseases like diabetes and blood pressure. For them, indeed, highly trained technicians and self-disciplined patients are still required to run measurements or deliver drugs as needed, impeding accurate timely interventions.

A promising solution to address these healthcare needs lies in closed-loop WI systems, integrating smart sensing-controller-therapeutic interaction, as shown in Figure 1(a). This revolutionary paradigm combines accurate sensing modalities with power transfer technology, data communication infrastructure, and machine learning algorithms, enhancing theragnostics. Skin-worn tattoos, patches, and textiles with wearable and implantable technology, along with actuating systems like brain and muscle stimulators or drug injectors, enable uninterrupted monitoring and immediate on-demand corrective therapies.

Microneedle (MN)-based patches, shown in Figure 1(b), are part of WI systems, offering minimally-invasive analyte monitoring and drug delivery over several weeks [6,7]. These patches with short microneedles (a few hundred micrometers) per cm^2 can absorb analyte molecules or deliver drugs into the dermis. Compared to traditional hypodermic needles, MNs are less invasive and less painful due to fewer pain receptors in the dermis [8,9]. Moreover, the interstitial fluid (ISF) within the dermis contains valuable biomarkers like glucose, lactate, sodium ions, and others [10,11].

The combination of disease diagnostics and drug delivery makes MN platforms ideal for closed-loop applications such as glycemic management and insulin therapy [12–14]. In traditional 'open-loop' operations, a patient performs glucose measurements and insulin pump therapy. In contrast, a smart MN patch integrates autonomous glucose measurement, data transmission to a controller algorithm, and autonomous therapeutic insulin delivery, forming a more efficient 'closed-loop' system.

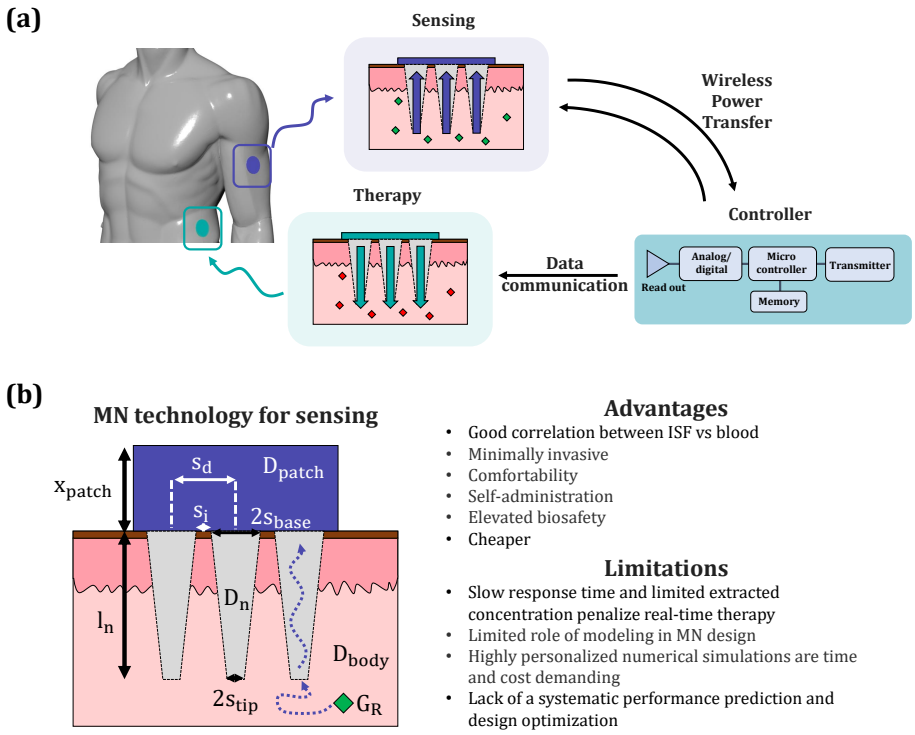

Figure 1. (a) Illustration of a closed-loop system (sensing, controller,therapy) integrating microneedle (MN) technology for a wearable and implantable (WI) device. (b) Illustration of geometric and physical properties of a MN-based patch, given an analyte concentration of interest in the dermis G_R. On the right, advantages and current limitations of the MN technology. l_n, s_{tip}, s_{base}, s_d are the MN length, tip and base half widths, inter-distance, respectively. x_{patch} is the patch thickness, and D_{patch}, D_n, D_{body} are the analyte diffusivity in patch, MN and body, respectively.

2. Challenges and limitations of MN technology

The number of publications in MN-related areas has been growing exponentially over the past 20 years, with more than 80% of these publications focusing on experimental systems and fabrication protocols [15]. Despite significant progress in the field, the current

design and optimization of MN systems involve costly and time-consuming iterative design-of-experiments. Researchers have explored a range of MN technologies, such as porous, swellable, and dissolvable platforms, alongside traditional hollow MNs, to achieve continuous monitoring with minimized sensor response delay and maximize the extracted concentration. If exploited, the utilization of numerical analysis tools, such as finite element methods with COMSOL Multiphysics software, has limitations in efficiently exploring the vast design space associated with MN geometry and material parameters. The lack of universal scaling functions derived from numerical simulations makes it challenging to transfer insights from one design to another, hindering systematic design and optimization of MN-based systems.

While a theory for therapeutic drug delivery has been developed [16], a comprehensive physics-based model for sensing optimization mediated by MNs is still missing. Without such a theory, it is difficult, if not impossible, to minimize response time and maximize extracted analyte concentration (limit of detection, LOD) for an optimized and efficient closed-loop system.

To address this gap, our work focuses on developing a generalized physics-based model for the in-vivo operation of hollow, porous, and swellable (P-S) MN-based patches. Through validation against numerical simulations and experimental data, our theory establishes the foundation for the MN-related framework and provides strategies for designing and optimizing MN systems within the closed-loop theragnostic scenario. Moreover, the generality of the MN scaling theory makes it applicable to a broader range of applications, including electrochemical or optical sensors, enzymatic or non-enzymatic processes, in-vitro and in-vivo measurements, sensing, and actuation mechanisms.

3. A scaling theory of response time and limit of detection

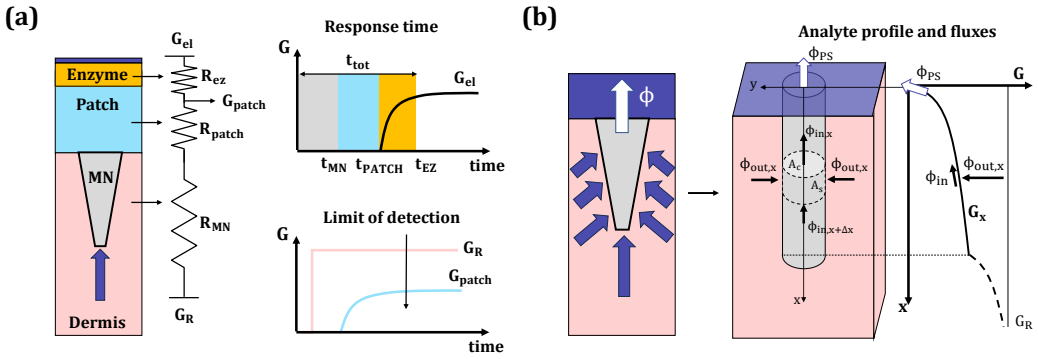

Figure 2. (a) Illustration of an hollow MN-based enzymatic sensor, and corresponding modeling in terms of electrical circuitry. Hollow MNs suffer from an intrinsic lag time t_{tot}; the total response is the sum of transport time across the MN (t_{MN}), sensor patch (t_{PATCH}) and enzyme kinetics (t_{EZ}). Also, given a fixed G_R (pink line), the accumulated analyte concentration in the patch (blue line, G_{patch}) is strongly suppressed, degrading the limit of detection (LOD). (b) Illustration of porous and swellable (P-S) cylindrical MN absorbing biofluid across the later surface, and corresponding modeling. We applied a balance of fluxes for a MN slice at distance x from base aperture to derive the the theory of analyte profile G_x (shown on the right) and extracted flux Φ_{PS}.

3.1. Specific design challenges

- Wearable sensing devices require continuous and effective operation, necessitating real-time tracking of analyte concentrations. However, integrating MNs into wearable patches poses challenges due to analyte diffusion from the interstitial fluid (ISF) to the sensing site. This diffusion causes inherent delays in sensor response (response time) and reduces the detectable analyte concentration (LOD) (Figure 2(a)), hindering an immediate closed-loop therapeutic response.

- Integrating fluid-absorbing MNs into electrochemical enzyme-based patches for on-site analysis adds complexity. Decoupling the impact of individual MN and enzymatic parameters on overall sensor performance proves to be a challenging task.
- Unlike hollow MNs, which absorb ISF across their tip aperture, P-S MNs enhance ISF absorption across their lateral surface, leading to a significant reduction in response time and increased extracted analyte concentration (Figure 2). However, a theory comparing different MN technologies and quantifying this enhancement is currently missing.

3.2. Theoretical framework of hollow microneedles

First, we derive a generalized framework to quantify the geometry-dependent response delay and LOD observed in hollow-type MN sensors. Here, the MNs are integrated in an enzymatic wearable patch with sensing site (electrode) on the upper end of the patch, as shown in Figure 2(a). We model the analyte extraction across MN tip and base as ion uptake by bacteria and gas flow across leaves stomata [17] and molecule transport along MN length as spreading resistance of a point contact [18]. It can be shown the overall response time t_{tot} is the sum of individual contributions from MN, patch and enzymatic reaction:

$$t_{tot} = t_{MN} + t_{PATCH} + t_{EZ}, \tag{1}$$

where t_{MN} and t_{PATCH} are the turn-on delay times of analyte transport through the MN and sensor patch, and t_{EZ} is the effective time resulting from diffusion and reaction in the enzyme layer, shown in Figure 2(a). To quantify the time components, we approximate each sensor domain as a diffusive resistor R $[s \cdot m^{-3}]$ and multiply it by the corresponding transported ISF volume V [19]. To generalize the theory, we express the geometry-dependent components of (1), namely $l_n, s_{base}, s_{tip}, s_i$, in terms of scaled variables, $r_T = \frac{l_n}{s_{tip}}$, $r_B = \frac{l_n}{s_{base}}$, $r_i = \frac{l_n}{s_i}$, where l_n, s_{tip}, s_{base} are the MN length, half width of MN tip, and base apertures, respectively, s_i is the MN inter-base distance:

$$t_{MN} = R_{base}V_{base} + R_nV_n + R_{tip}V_{tip} = f(r_T, r_B, r_i, D_{body}, D_n, D_{patch}) \tag{2}$$

$$t_{PATCH} = R_{patch}V_{patch} = f(x_{patch}, D_{patch}) \tag{3}$$

$$t_{EZ} = \text{diffusion} - \text{limited } (t_{MN}, t_{PATCH}) \text{ vs reaction} - \text{limited (reaction rates)} \tag{4}$$

Here x_{patch} is the patch thickness, D_{body}, D_n, D_{patch} are the analyte effective diffusivity in dermis, MN and patch, respectively. The parameter t_{EZ} results from the competition of analyte supply from the dermis (transport-limited) and enzyme kinetics (reaction rates).

Second, we quantify the averaged analyte concentration extracted in the patch (G_{patch}), given a fixed concentration in the dermis G_R, see Figure 2(a). Regardless of the transduction mechanism (colorimetric, electrochemical, etc.), the accumulated G_{patch} is a critical parameter related to the minimum signal level set by noise limit (LOD); since G_{patch} may degrade below the noise limit along the diffusive path to the sensing site, the sensor may not register analyte fluctuations in the skin and, so, fail to deliver the appropriate drug amount. To derive G_{patch}, we assume steady state conditions, and apply flux continuity among the enzyme, patch and MN [19]:

$$\frac{G_{patch}}{G_R} \propto \frac{R_{ez} + \frac{R_{patch}}{2}}{R_{base} + R_n + R_{tip}} \tag{5}$$

3.3. Theoretical enhancement of porous and swellable microneedles

For a faster closed-loop sensing and therapy, several approaches have been experimentally proposed, including the integration of P-S MNs in wearable patches [6,7,20,21]. Here, we derive a universal scaling relationship for P-S MNs, and quantify their flux enhancement against hollow MNs. Ideally, given an arbitrary MN technology, the absorbing flux across the MN base aperture should be maximized for superior performance; an higher flux would

absorb higher analyte concentration in a shorter time to satisfy timely monitoring restrictions and minimum signal-to-noise ratio levels.

Although the theory can be generalized for an arbitrary geometry, we assume a cylindrical, homogeneous, isotropic MN, as shown in Figure 2(b). First, we apply a flux balance in a slice of the MN at a distance x from the base:

$$\Phi_{in,x+\Delta x}A_c - \Phi_{in,x}A_c + \Phi_{out,x}A_s = 0, \tag{6}$$

where the concentration-dependent flux Φ is the gradient of analyte concentration, and A_c and A_s are the crossectional and lateral surface areas of the slice. The steady state solution of (6) gives the analyte profile G_x within the MN, assuming a fully absorbing MN base aperture ($G_{x=0} = 0$), see Figure 2(b):

$$\frac{G_x}{G_R} = 1 - \frac{\cosh(m(l_n - x)) + H\sinh(m(l_n - x))}{\cosh(ml_n) + H\sinh(ml_n)} \tag{7}$$

where s is the MN radius, $m \equiv \sqrt{\frac{2h_T}{sD_n}}$ with h_T being an empirical geometry-dependent coefficient regulating analyte transfer between MN and dermis, and $H = \frac{h_T}{mD_n}$.

Second, to evaluate the extraction efficiency of a P-S MN (Γ_{PS}), we normalize the flux at the base of MN aperture ($\Phi \propto D_n\frac{dG_x}{dx}$ at $x = 0$):

$$\Gamma_{PS} = r_h\frac{\sinh(r_h) + \frac{1}{2}r_g r_h\cosh(r_h)}{\cosh(r_h) + \frac{1}{2}r_g r_h\sinh(r_h)} \tag{8}$$

where

$$r_h = ml_n \equiv \sqrt{h_T/\left(\frac{sD_n}{2l_n^2}\right)} \tag{9}$$

$$r_g \equiv \frac{s}{l_n} \tag{10}$$

Here, the parameter r_h encapsulates geometric and physical properties of MN and surrounding environment, therefore dictating the P-S ability to absorb analytes from the dermis. To compare the performance of P-S and hollow technology, we derive a similar relationship for hollow MNs at the base aperture of the MN:

$$\Gamma_H \approx \frac{1}{1 + \frac{D_n}{D_{body}}r_g} \tag{11}$$

The ratio Γ_{PS}/Γ_H shows the theoretical enhancement in extracting flux between P-S MNs and hollow MNs.

4. Results

4.1. Impact on response time and limit of detection

Validated against COMSOL-based simulations, Figure 3(a) shows the impact of l_n on response time (left, (1)) and limit of detection (right, (5)) for an hollow MN-based patch. As expected, the theory predicts a tens of minutes to tens of hours lag time affecting the sensing operation of MN-based patches, depending on sensor design. Diffusion time across the patch (t_{PATCH}, (3)) and enzyme-related delay (t_{EZ}, (4)) sets the critical limit of the performance. Overall, a longer MN would increase the transport time, degrading the closed-loop efficiency and suppressing the absorbed analyte concentration. Although not reported, a similar approach can be applied to predict the impact of other geometric and physical properties (MN apertures, MN material and patch thickness) on sensor performance.

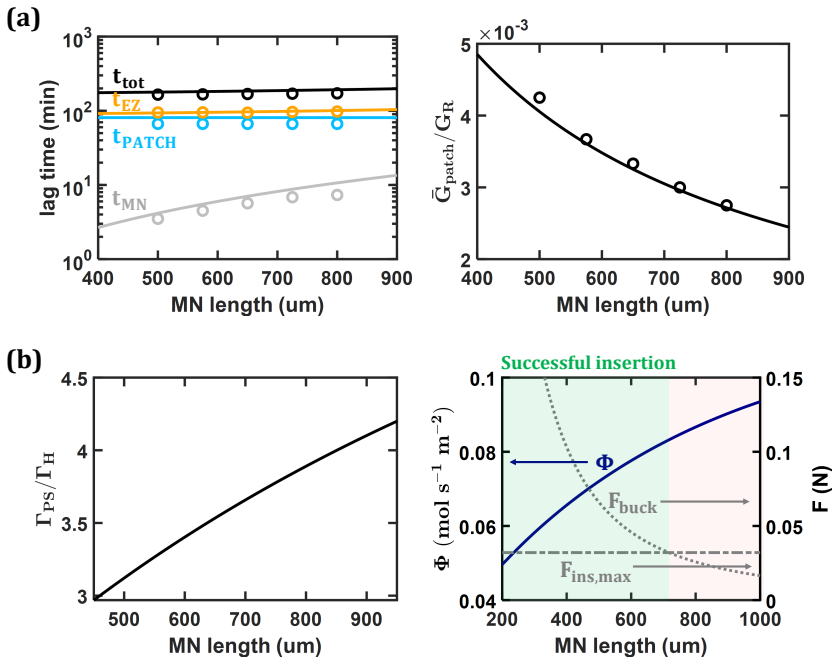

Figure 3. (a) Numerical validation of hollow MNs. Impact of MN length on (left) individual components of total response time and on (right) absorbed glucose concentration. Solid line is the theory, circles are numerical results. (b) Analytical prediction for P-S MNs. Impact of MN length on (left) enhancement factor between P-S and hollow MNs and (right) on trade-off between sensor performance (absorbed flux, blue line) and mechanical requirements (dotted and dashed grey lines).

4.2. Enhancement and limitations for porous and swellable microneedles

Figure 3(b) shows the impact of l_n on the enhancement factor between P-S and hollow MNs ((8), (11), left) and on the trade-off between extracted flux and mechanical constraints for a P-S MN (right). Unlike a hollow MN, a P-S MN benefits from a longer MN, because of the enhanced surface area absorbing biofluid, see Figure 3(a) (right). The enhancement factor introduced by l_n is between 3 and 4; yet, by varying other geometric and physical variables (MN radius, diffusivity, etc.), it can be shown it can achieve a factor of 6. Despite the significant benefits in performance, P-S MNs suffer from a weaker mechanical strength, limiting their skin insertion. Figure 3(b) shows the trade-off between performance and mechanical constraints defines a 'window design' for P-S MNs. To mechanically succeed, a margin of mechanical safety ($F_{ins,max} < F_{buck}$, buckling limit higher than the maximum force supported by the MN) should be guaranteed, see [22]. While a longer MN maximizes the extracting flux Φ, it may cause mechanical failure ($F_{ins,max} > F_{buck}$); therefore, there exists an optimized length satisfying both performance and mechanics at $F_{ins,max} = F_{buck}$.

5. Conclusion

We developed a generalized theoretical framework for hollow and P-S MNs integrated into wearable patches as part of a comprehensive predictive model for personalized, autonomous, and independent theragnostics. Our theory quantifies sensor performance, including response time and extracted analyte concentration, based on geometric and physical properties of the sensor. We also identified the fundamental limitations of hollow MNs and predicted an enhancement factor introduced by P-S MNs, albeit with a trade-off of weaker mechanical strength.

The model can be generalized to analyze novel MN technologies for an improved response time. For instance, the integration of sensing sites (electrodes) within MNs accelerates the detection by reducing transport time [23]. Despite potential degradation due

to biofouling, the approaches involving functionalized MN surfaces reduce the response time by directly exposing sensing sites to analyte fluctuations in the dermis [24].

For a comprehensive analysis, the model should incorporate considerations on mechanical failure, inflammation, and biocompatibility-related concerns of MNs. More generally, by including a sensing-to-therapy algorithm, and a theory for drug delivery, we would be able to provide a comprehensive framework for a systematic optimization of MN-based systems.

Funding: This work was funded by Eli Lilly & Company. We thank Michelle Pearson for coordinating the operations between Prof. Alam group and Eli Lilly & Company. The work was also supported by the Jai N. Gupta Endowed Chair Fund for Prof. Alam.

Acknowledgments: The authors gratefully acknowledge discussion with Jongcheon Lim, Jim Nolan, Emilee Madsen, Yumin Dai, Profs. Chi Hwan Lee (Purdue University), Hugh Lee (Purdue University), Jacqueline C. Linnes (Purdue University).

Conflicts of Interest: The authors declare no conflict of interest.

References

1. Fratus, M.; Alam, M.A. Universal scaling theory of electrochemical immunosensors: An analytical approach to define and compare performance metrics. *Applied Physics Letters* **2023**, *122*, [https://pubs.aip.org/aip/apl/article-pdf/doi/10.1063/5.0133669/16734551/054102_1_online.pdf]. 054102, https://doi.org/10.1063/5.0133669.
2. Heikenfeld, J.; Jajack, A.; Feldman, B.; Granger, S.W.; Gaitonde, S.; Begtrup, G.; Katchman, B.A. Accessing analytes in biofluids for peripheral biochemical monitoring. *Nature Biotechnology* **2019**, *37*, 407–419. https://doi.org/10.1038/s41587-019-0040-3.
3. de-la Fuente-Robles, Y.M.; Ricoy-Cano, A.J.; Albín-Rodríguez, A.P.; López-Ruiz, J.L.; Espinilla-Estévez, M. Past, Present and Future of Research on Wearable Technologies for Healthcare: A Bibliometric Analysis Using Scopus. *Sensors* **2022**, *22*. https://doi.org/10.3390/s22228599.
4. Friedel, M.; Thompson, I.A.P.; Kasting, G.; Polsky, R.; Cunningham, D.; Soh, H.T.; Heikenfeld, J. Opportunities and challenges in the diagnostic utility of dermal interstitial fluid. *Nature Biomedical Engineering* **2023**. https://doi.org/10.1038/s41551-022-00998-9.
5. Alam, M.A.; Saha, A.; Fratus, M. Reliable sensing with unreliable sensors: Rethinking the theoretical foundation of field-deployed wearable/implantable/environmental sensors. *Innovation and Emerging Technologies* **2022**, *09*.
6. Zhang, X.; Gan, J.; Fan, L.; Luo, Z.; Zhao, Y. Bioinspired Adaptable Indwelling Microneedles for Treatment of Diabetic Ulcers. *Advanced Materials* **2023**, *35*, 2210903, [https://onlinelibrary.wiley.com/doi/pdf/10.1002/adma.202210903]. https://doi.org/https://doi.org/10.1002/adma.202210903.
7. Sang, M.; Cho, M.; Lim, S.; Min, I.S.; Han, Y.; Lee, C.; Shin, J.; Yoon, K.; Yeo, W.H.; Lee, T.; et al. Fluorescent-based biodegradable microneedle sensor array for tether-free continuous glucose monitoring with smartphone application. *Science Advances* **2023**, *9*, eadh1765, [https://www.science.org/doi/pdf/10.1126/sciadv.adh1765]. https://doi.org/10.1126/sciadv.adh1765.
8. Ribet, F.; Bendes, A.; Fredolini, C.; Dobielewski, M.; Böttcher, M.; Beck, O.; Schwenk, J.M.; Stemme, G.; Roxhed, N. Microneedle Patch for Painless Intradermal Collection of Interstitial Fluid Enabling Multianalyte Measurement of Small Molecules, SARS-CoV-2 Antibodies, and Protein Profiling. *Advanced Healthcare Materials* **2023**, *12*, 2202564, [https://onlinelibrary.wiley.com/doi/pdf/10.1002/adhm.202202564]. https://doi.org/https://doi.org/10.1002/adhm.202202564.
9. Xu, J.; Yang, B.; Kong, J.; Zhang, Y.; Fang, X. Real-Time Monitoring and Early Warning of a Cytokine Storm In Vivo Using a Wearable Noninvasive Skin Microneedle Patch. *Advanced Healthcare Materials* **2023**, *12*, 2203133, [https://onlinelibrary.wiley.com/doi/pdf/10.1002/adhm.202203133]. https://doi.org/https://doi.org/10.1002/adhm.202203133.
10. Müller, M.; Cascales, J.P.; Marks, H.L.; Wang-Evers, M.; Manstein, D.; Evans, C.L. Phosphorescent Microneedle Array for the Measurement of Oxygen Partial Pressure in Tissue. *ACS Sensors* **2022**, *7*, 3440–3449, [https://doi.org/10.1021/acssensors.2c01775]. PMID: 36305608, https://doi.org/10.1021/acssensors.2c01775.
11. Himawan, A.; Vora, L.K.; Permana, A.D.; Sudir, S.; Nurdin, A.R.; Nislawati, R.; Hasyim, R.; Scott, C.J.; Donnelly, R.F. Where Microneedle Meets Biomarkers: Futuristic Application for Diagnosing and Monitoring Localized External Organ Diseases. *Advanced Healthcare Materials* **2023**, *12*, 2202066, [https://onlinelibrary.wiley.com/doi/pdf/10.1002/adhm.202202066]. https://doi.org/https://doi.org/10.1002/adhm.202202066.
12. Ghoreishizadeh, S.S.; Moschou, D.; McBay, D.; Gonalez-Solino, C.; Dutta, G.; Di Lorenzo, M.; Soltan, A. Towards self-powered and autonomous wearable glucose sensor. In Proceedings of the 2018 25th IEEE International Conference on Electronics, Circuits and Systems (ICECS), 2018, pp. 701–704. https://doi.org/10.1109/ICECS.2018.8618022.
13. Boughton, C.K.; Hovorka, R. New closed-loop insulin systems. *Diabetologia* **2021**, *64*, 1007–1015. https://doi.org/https://doi.org/10.1007/s00125-021-05391-w.

14. Doyle, Francis J., I.; Huyett, L.M.; Lee, J.B.; Zisser, H.C.; Dassau, E. Closed-Loop Artificial Pancreas Systems: Engineering the Algorithms. *Diabetes Care* **2014**, *37*, 1191–1197, [https://diabetesjournals.org/care/article-pdf/37/5/1191/621467/1191.pdf]. https://doi.org/10.2337/dc13-2108.
15. Yadav, P.R.; Han, T.; Olatunji, O.; Pattanayek, S.K.; Das, D.B. Mathematical Modelling, Simulation and Optimisation of Microneedles for Transdermal Drug Delivery: Trends and Progress. *Pharmaceutics* **2020**, *12*. https://doi.org/10.3390/pharmaceutics12080693.
16. Avila, R.; Li, C.; Xue, Y.; Rogers, J.A.; Huang, Y. Modeling programmable drug delivery in bioelectronics with electrochemical actuation. *Proceedings of the National Academy of Sciences* **2021**, *118*, e2026405118, [https://www.pnas.org/doi/pdf/10.1073/pnas.202640 https://doi.org/10.1073/pnas.2026405118.
17. Berg, H.C. *Random Walks in Biology*; Princeton University Press: Princeton, 2018. https://doi.org/doi:10.1515/9781400820023.
18. Karmalkar, S.; Mohan, P.V.; Nair, H.P.; Yeluri, R. Compact Models of Spreading Resistances for Electrical/Thermal Design of Devices and ICs. *IEEE Transactions on Electron Devices* **2007**, *54*, 1734–1743. https://doi.org/10.1109/TED.2007.899371.
19. Fratus, M.; Lim, J.; Nolan, J.; Madsen, E.; Dai, Y.; Lee, C.H.; Linnes, J.C.; Lee, H.; Alam, M.A. Geometry-defined Response Time and Sensitivity for Microneedle-based Amperometric Sensors. *IEEE Sensors Journal* **2023**, pp. 1–1. https://doi.org/10.1109/JSEN.2023.3277425.
20. Zhang, J.; Li, H.; Albakr, L.; Zhang, Y.; Lu, A.; Chen, W.; Shao, T.; Zhu, L.; Yuan, H.; Yang, G.; et al. Microneedle-enabled therapeutics delivery and biosensing in clinical trials. *Journal of Controlled Release* **2023**, *360*, 687–704. https://doi.org/https://doi.org/10.1016/j.jconrel.2023.07.023.
21. Li, X.; Xu, X.; Wang, K.; Chen, Y.; Zhang, Y.; Si, Q.; Pan, Z.; Jia, F.; Cui, X.; Wang, X.; et al. Fluorescence-Amplified Origami Microneedle Device for Quantitatively Monitoring Blood Glucose. *Advanced Materials* **2023**, *35*, 2208820, [https://onlinelibrary.wiley.com/doi/pdf/10.1002/adma.202208820]. https://doi.org/https://doi.org/10.1002/adma.202208820.
22. Kashaninejad, N.; Munaz, A.; Moghadas, H.; Yadav, S.; Umer, M.; Nguyen, N.T. Microneedle Arrays for Sampling and Sensing Skin Interstitial Fluid. *Chemosensors* **2021**, *9*. https://doi.org/10.3390/chemosensors9040083.
23. Parrilla, M.; Vanhooydonck, A.; Johns, M.; Watts, R.; De Wael, K. 3D-printed microneedle-based potentiometric sensor for pH monitoring in skin interstitial fluid. *Sensors and Actuators B: Chemical* **2023**, *378*, 133159. https://doi.org/https://doi.org/10.1016/j.snb.2022.133159.
24. Teh, F.; Teymourian, H.; Wuerstle, B.; Kavner, J.; Patel, R.; Furmidge, A.; Aghavali, R.; Hosseini-Toudeshki, H.; Brown, C.; Zhang, F.; et al. An integrated wearable microneedle array for the continuous monitoring of multiple biomarkers in interstitial fluid. *Nature Biomedical Engineering* **2022**, *6*, 1–11. https://doi.org/10.1038/s41551-022-00887-1.